Zhang, Shuzhong; Minav, Tatiana; Pietola, Matti; Kauranne, Heikki; Kajaste, Jyrki

The effects of control methods on energy efficiency and position tracking of an electro-hydraulic excavator equipped with zonal hydraulics

Published in:
Automation in Construction

DOI:
10.1016/j.autcon.2019.01.003

Published: 01/04/2019

Document Version
Publisher's PDF, also known as Version of record

Please cite the original version:
Zhang, S., Minav, T., Pietola, M., Kauranne, H., & Kajaste, J. (2019). The effects of control methods on energy efficiency and position tracking of an electro-hydraulic excavator equipped with zonal hydraulics. *Automation in Construction*, *100*, 129-144. https://doi.org/10.1016/j.autcon.2019.01.003

Automation in Construction 100 (2019) 129–144

Contents lists available at ScienceDirect

Automation in Construction

journal homepage: www.elsevier.com/locate/autcon

The effects of control methods on energy efficiency and position tracking of an electro-hydraulic excavator equipped with zonal hydraulics

Shuzhong Zhang[a,b,*], Tatiana Minav[b,c], Matti Pietola[b], Heikki Kauranne[b], Jyrki Kajaste[b]

[a] School of Mechanical and Automotive Engineering, Fujian University of Technology, 350118 Fuzhou, China
[b] Department of Mechanical Engineering, Aalto University, PO Box 14300, 00076 Espoo, Finland
[c] Saint-Petersburg Electrotechnical University ETU "LETI", ul. Professora Popova 5, 197376 St. Petersburg, Russia

ARTICLE INFO

Keywords:
Direct driven hydraulics
Zonal hydraulics
Energy efficiency
Position tracking
Flow-rate-matching feedforward control
Pump/motor model
Electro-hydraulic excavator
Working cycle

ABSTRACT

Compared to conventional central hydraulic systems still typically used in most off-road machinery, the main advantages of zonal hydraulics are lower pressure losses, lower power demand, and thus, lower energy consumption on a system level and easy automatisation. In this case study, zonal hydraulics is realised with Direct Driven Hydraulics (DDH), and it is implemented as a replacement for the conventional centralised hydraulic system of a micro excavator. A simulation model for the front attachment of the excavator with three individual DDH units is presented. The proposed model of a single DDH unit was partially validated with a standalone test setup. Various common working cycles, such as digging and dumping with differing payloads and levelling, were adopted for this simulation study. Two controllers—a conventional proportional-integral-derivative (PID) controller and a flow-rate-matching feedforward plus PID controller—were designed for each DDH unit. Thereafter, detailed comparisons were provided, consisting of energy consumption, energy efficiency and position tracking performance between the two controllers. The results showed that the proposed feedforward plus PID controller had better performance than a conventional PID in the studied case. By adopting this controller, higher system energy efficiency (improved by 11–24% without regeneration and by 8–28% when considering regeneration) and better position tracking performance (root mean square tracking error and max errors lowered by 20–87% and 35–83%, respectively) were achieved simultaneously. Therefore, this work can be applied to zonal hydraulics to facilitate the electrification and automatisation of construction machinery.

1. Introduction

High and rising energy (fuel) prices, the demand to reduce fossil energy sources and new emission rules have directed research towards improving the energy efficiency and environmental friendliness (less pollution) of different work machines as a matter that urgently needs to be addressed. For instance, off-road machinery is responsible for approximately 60% of the CO_2 emissions produced by different construction machines. Regarding excavators, the object of research in this paper, several studies related to improving the energy efficiency by hybridisation [1–4] and electrification [5–8] have been published; in addition, some excavator manufacturers have already applied these technologies in their products. For instance, 1) regarding hybridisation: in [9], a survey demonstrated that various hybrid electric systems have been introduced into construction machinery by researchers and manufacturers; compared with ordinary excavators, such machinery can obtain > 20% energy-saving efficiency. In the meantime, it was pointed out that a pure electric transmission system based on a battery or fuel cell may be the best choice for future construction machinery. For instance, 2) regarding electrification: Sennebogen has been implementing material handlers with electric drives that receive their electric supply from a power grid for over 25 years and has reduced operating costs by up to 50% [6]. JCB has unveiled its first-ever electric excavator by replacing the diesel engine with a 48 V electrical driveline with the latest-generation automotive battery cells, the 19C-1 *E*-TEC mini-excavator, which is the '*quietest machine in its range*' (external noise lower by 7dBA) and delivers '*zero emissions*' [5]. Volvo Construction Equipment has also recently introduced the EX2 (a fully electric compact excavator that delivers zero emissions). The combustion engine and hydraulic system have been replaced with two lithium ion batteries and electromechanical linear actuators, respectively [7]. In [10], an electric hydraulic excavator configuration was proposed to improve the overall energy efficiency and eliminate emissions; it consisted of an independent metering-in and metering-out hydraulic system and a

* Corresponding author at: College of Mechanical and Automotive Engineering, Fujian University of Technology, 350118 Fuzhou, China.
E-mail address: shuzhong_zhang@outlook.com (S. Zhang).

https://doi.org/10.1016/j.autcon.2019.01.003
Received 5 July 2018; Received in revised form 24 December 2018; Accepted 7 January 2019

displacement variable pump driven by a speed variable electric motor with an external electric supply.

Despite the achievements in electrification in excavators, converting the combustion engine into an electric motor powered by batteries or an electric supply, limited improvements with respect to the powertrain for pure electric construction machinery, were only made to the working hydraulics to improve the system's energy efficiency and to extend the operation time of the batteries. Another study [11] proposed using an automatic idle speed control system with a hydraulic accumulator for a pure electric excavator, and, compared to a system without idle speed control, the energy savings of the proposed system is approximately 36.1%. Usually when developing an automatic operation for construction machinery, various possible control methods can be implemented [12], such as position, compliance and feedforward control, artificial intelligence; likewise, reinforcement learning methods are attracting the attention of researchers. However, limited studies have been conducted that combine a position control and energy savings point of view.

In our previous study [13,14], the concept of zonal hydraulics was introduced in an excavator and a mining loader, which has been used in the aircraft industry and realised with Electrohydrostatic Actuator (EHA) systems. Compared to the conventional central hydraulic systems still typically used in most off-road machinery, the main advantages of zonal hydraulics are lower pressure losses, lower power demand and, thus, lower energy consumption on a system level and easy automatisation (due to the fact that each actuator can be independently controlled). To facilitate the electrification process, unattended operation and automatisation of off-road machinery, a zonal hydraulics realised with Direct Driven Hydraulics (DDH) (one configuration of EHA) was introduced for the working hydraulics of off-road machinery. Each DDH unit was comprised of one electric motor, one servo drive, two pump/motors, one hydraulic accumulator and one asymmetrical cylinder. In [13], the simulation result showed that the energy efficiency of the micro excavator with DDH units was 71%, but only 20% with a load sensing system.

However, in [13] the mechanical model did not consider the extra weights and mounting points of the three DDH units; the pump/motor volumetric efficiency models contained only pressure difference, but not the rotating speed, and the hydro-mechanical efficiencies were set to be constant; the friction models of the cylinders were not identified via measurement. In addition, the position tracking performance of DDH units when used with an excavator has not been studied yet. Therefore, this paper presents a case study on the effects of control methods regarding the energy efficiency and tracking performance of an electro-hydraulic excavator equipped with zonal hydraulics—as a case study by means of a significantly improved simulation model from the tracking performance and energy consumption points of view.

The rest of the paper is organised as follows. The test case is introduced in Section 2, while Section 3 describes the proposed electro-hydraulic model for this study case in detail. Controller designs are explained in Section 4. Tracking performance and energy consumption are evaluated and analysed in Section 5. Finally, Sections 6 and 7 contain a discussion and concluding remarks.

2. Test case

2.1. Overview of the test arrangements

In this case study, the research object is the JCB micro excavator (Fig. 1) available in the Fluid Power Laboratory at Aalto University.

The original hydraulic system and the prime mover of the micro excavator have been previously modified [15]. A stack of electronically controlled proportional valves was installed in parallel to the original manual HC-D9 control valves. The diesel engine (net power 12.7 kW) was removed and replaced with a 10 kW electric motor plus a battery pack.

Fig. 1. Photograph of the JCB excavator.

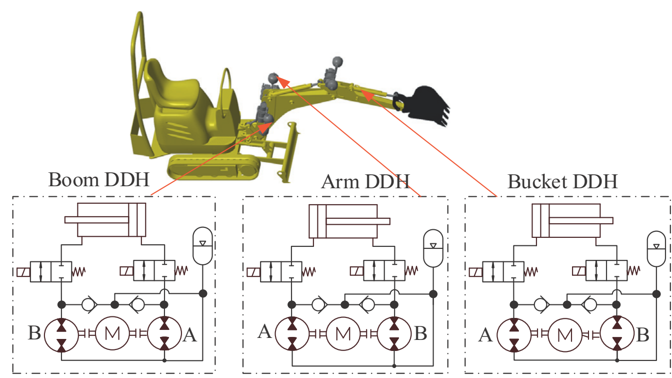

Fig. 2. Zonal excavator topology with three DDH units.

In this study, the conventional centralised hydraulic system is proposed to be replaced with localised zonal hydraulics, namely three DDH units for the boom, arm and bucket, respectively, as presented in Fig. 2.

For the boom, arm and bucket cylinders, the effective area ratios R_{ideal} of the rod side to the piston are given by the excavator manufacturer. Hence, the displacement ratio R_{real} of two pump/motors in each DDH unit should be as close to R_{ideal} as possible. When the sizing deviation $R_{\text{deviation}}$ between R_{ideal} and R_{ideal} is > 2%, a flow imbalance compensation strategy is required [16,17].

The simplicity of the gear pump design translates into higher reliability compared to other positive displacement pumps that use a more complex design [18]. High-speed rotation, a simple structure, low cost and higher reliability of the gear pump make it particularly suitable for DDH. In this case, in order to reduce the mechanical inertia of pumps (to obtain better dynamics and higher acceleration capabilities) and lower the energy consumption caused by the extra weight of DDH units by using smaller gear pump/motors instead of piston pumps, small-sized external gear motors (from the HYDAC MGE101 and MGE102 series) with desired displacement ratios and low weights are chosen for all three cylinders and operate as four-quadrant pumps [19]. Table 1 presents the three pairs of selected hydraulic motors for the boom, arm and bucket DDH units. As a result, the sizing deviations of DDH for the boom, arm and bucket were 0.13%, 0.02% and 0.02%, respectively. According to [16,17], when the sizing deviation is < 2%, DDH units for the arm and bucket can function normally without a flow compensation strategy. Additionally, on/off valves were selected for position holding and a low-pressure accumulator was installed as a substitute for the tank in each DDH unit, as shown in Fig. 2. Furthermore, two check valves are used to avoid cavitation in the transmission

Table 1
Parameters of cylinders and pump/motors [19].

	Cylinder [mm]	Displacement ratio			Pump/motor B/A	
		R_{ideal}	R_{real}	$R_{deviation}$	Displacement [mL/r]	Weight [kg]
Boom	60/30 × 325	0.750	0.749	0.13%	4.95/6.61	3.3/3.3
Arm	50/30 × 400	0.640	0.640	0.02%	4.27/6.67	1.1/1.3
Bucket	50/30 × 290	0.640	0.640	0.02%	4.27/6.67	1.1/1.3

Table 2
Parameters of hydraulic accumulators [20].

	Fully charged Volume [L]	Hydraulic accumulator			
		Capability [L]	Precharge pressure [MPa]	Maximum pressure [MPa]	Weight [kg]
Boom	0.230	0.7	0.10	0.175	4.0
Arm	0.283	0.7	0.10	0.201	4.0
Bucket	0.205	0.7	0.10	0.162	4.0

lines between the low-pressure side of the pump and the cylinder chamber caused by the leakage of the pump and sizing deviation.

The fluid volume differences between the full retraction and extension of three cylinders were calculated to be 0.230, 0.283 and 0.205 L for the boom, arm and bucket, respectively. Therefore, hydraulic accumulators with a nominal capability of 0.7 L were selected as reservoirs for all DDH units; their parameters are shown in Table 2. The minimum operating pressure of each accumulator was set at a precharge pressure of 0.1 MPa. The fluid volume differences calculated above are assumed to be fully charged for the corresponding accumulator in order to compute the maximum operating pressure of the accumulators. Due to working at low pressures, the charging process was simplified to an adiabatic process, and the adiabatic constant for nitrogen inside the accumulators was set to be 1.4.

2.2. Test cycles

In [21], the research concluded that tracked hydraulic excavators spent approximately 75% of their operating time performing an actual earthmoving task, including 15% for grading and 60% for digging. Furthermore, surveys conducted in this field suggested that the typical digging (digging and loading into a truck), trenching (trench digging and loading onto a pile) and levelling operations are the three most common duty cycles performed by excavators [21,22].

In this study, various types of operating cycles were performed to investigate the impact of the DDH with differing controllers on the system behaviour (position tracking, energy consumption, regeneration, velocity, oscillations). The selected operating cycles include an example of a typical digging cycle with changing payload adopted from Ref. [23] and a simulation cycle without payload, as defined by the Japan Construction Mechanization Association Standard (JCMAS) in 2007 [24].

2.2.1. Typical digging cycle with changing payload

Concerning the performance of the system with a load, a typical working cycle for the excavator in Ref. [23] was adopted as the input reference for the simulations. The relative positions of the three cylinders in this typical cycle are illustrated in Fig. 3a.

Normally, experienced operators have an average cycle time of 24.5 s to perform a similar trenching cycle with a 20-tonne excavator [25]. Therefore, in this paper a cycle time of 20 s was utilised for the one-tonne micro excavator. The typical earthmoving cycle consists of:

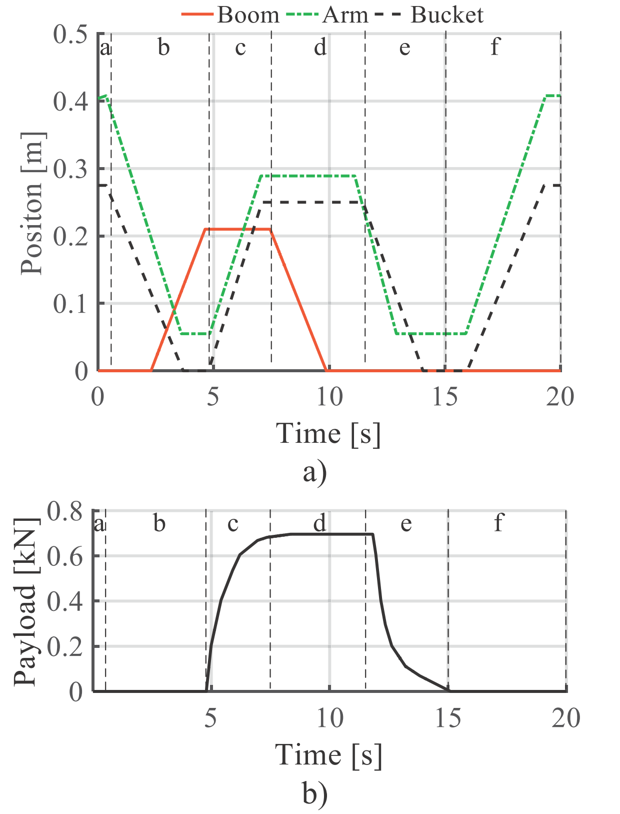

Fig. 3. a) Reference positions of the actuators in a typical digging cycle [19] and b) a simplified loading profile [23].

- a Starting from a minimum reach position;
- b Lowering the boom, lifting the arm and opening the bucket simultaneously;
- c Digging a bucketful of material;
- d Lifting the boom and swinging the upper structure 90 degrees;
- e Opening the bucket and discharging it;
- f Going back to the initial position.

The operating sequence of the typical digging cycle was obtained from Mechanics Explorers in MATLAB and is displayed in Fig. 4. In this study, the swing (rotating) motion of the upper structure is excluded due to a focus on the DDH units for the front attachment of the excavator.

A loading profile was created to simulate the changing payload; it

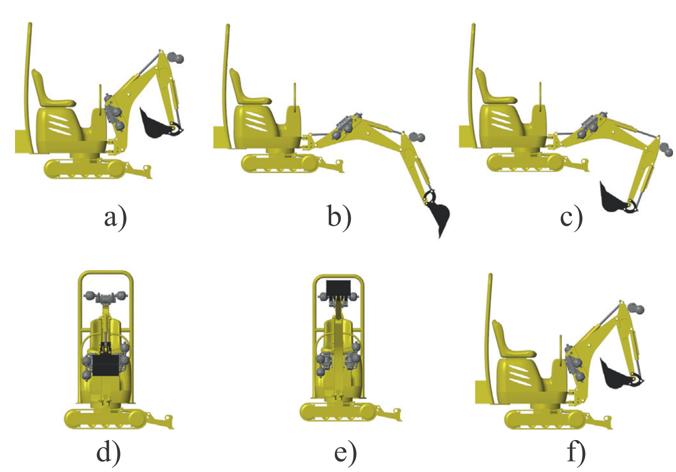

Fig. 4. Operating sequence of the typical digging cycle.

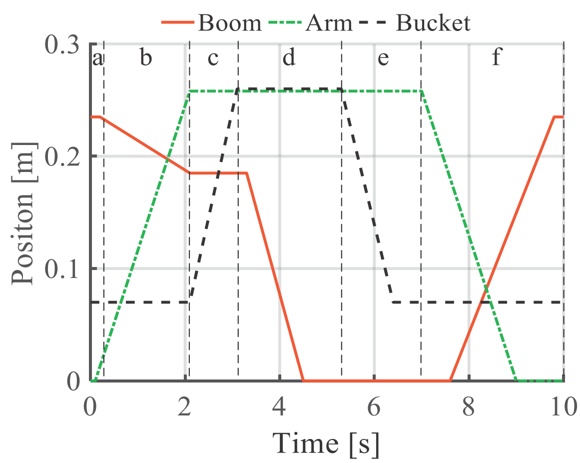

Fig. 5. Reference position of the actuators in the JCMAS digging cycle.

was designed to be similar to the one used in [26]. Fig. 3b demonstrates the simplified load. The bucket was modelled in PTC Creo 3.0 and filled with heaped material. The density of the material was defined as 2100 kg/m^3 (a value between the densities of clay and gravel) [27]. Since it is difficult to determine the terra-mechanical forces on the bucket during an actual digging cycle, a simplified, simulated, time-dependent payload of moving material was implemented [23].

2.2.2. JCMAS digging and levelling cycles

The JCMAS digging and levelling cycles were selected to avoid complex modelling of the earth and to realise as uniform conditions as possible for repeatable measurements, although they moved the bucket in the air and do not match the real-world test cycles [24].

The relative positions of the three actuators of the digging cycle are illustrated in Fig. 5, and the motions of the digging cycle are demonstrated in Fig. 6, including:

a Starting with maximum reach position;
b Horizontally pulling the bucket and the boom;
c Digging with the bucket;
d Swinging and lifting the boom;
e Dumping with the bucket;
f Returning to the initial position.

Since the reference bucket capability of the micro excavator (0.17 m^3) is under the minimum standard bucket capability (0.28 m^3) defined in the JCMAS 2007 standard, the digging depth and unloading height were scaled down to be 1 m and 0.65 m for the digging cycle according to JCMAS and the parameter of a one-tonne micro excavator, respectively. As with the levelling cycle, the swing motion of the excavator was excluded from the study.

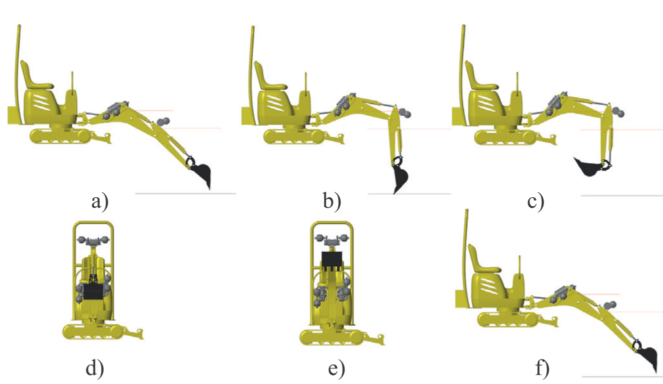

Fig. 6. Operating sequence of the JCMAS digging cycle [24].

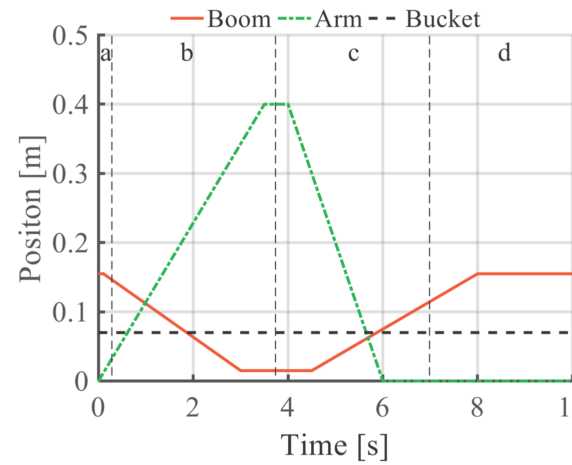

Fig. 7. Reference position of the actuators in the JCMAS levelling cycle.

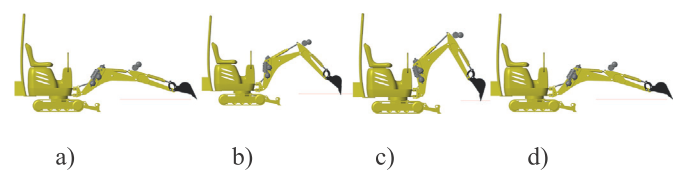

Fig. 8. Levelling cycle defined by JCMAS [24].

Fig. 7 and Fig. 8 demonstrate the relative positions and operating sequence of the levelling cycle, respectively:

a Starting with maximum reach position;
b Lifting the boom and extending the arm cylinder to do levelling;
c Lowering the boom and retracting the arm cylinder to return;
d Return to initial position.

3. Modelling and validation

This section introduces the modelling of DDH components and their validation. The multi-domain systems were modelled using MATLAB Simulink and SimMechanics, consisting of electrical, mechanical, hydraulic and control systems.

3.1. Electric drive

In this study, the model of a permanent-magnet synchronous motor (PMSM) based on [28] was realised in MATLAB/Simulink. The utilised model assumed the following simplifications:

- Machines have surface-mounted permanent magnets and non-salient poles.
- $i_d = 0$ motor vector control is utilised instead of a direct torque control, where a stator current space vector is utilised as $i_s = i_d + ji_q$ in the rotational dq coordinate and where i_q is the current on the q axis.

Therefore, the electromagnetic torque was calculated according to Eq. (1):

$$T_{em} = \frac{N_p}{2}\lambda_{fd}\, i_{dq}, \tag{1}$$

where $N_p = 3$ is the pole pairs, λ_{fd} is the flux linkage of the stator d winding and i_{sq} is the stator current on the q axis.

The dq transformation was utilised as part of the $i_d = 0$ vector motor control. The stator voltages in the dq transformation were calculated using Eqs. (2) and (3):

Table 3
PMSM characteristics [29].

Parameter	Value
Rated Speed	3000 rpm
Rated torque	8.1 N·m
Stall current	5.9 A
Rated power	2.54 kW
R_s - Resistance(phase)	2.02 Ω
L_s - Inductance(phase)	$13.27 \cdot 10^{-3}$H
Inertia	$9.0 \cdot 10^{-4}$ kg·m^2
Stall Torque	9.4 N·m
Peak torque	28.2 N·m
Weight	10 kg

$$v_{sd} = R_s i_{sd} - \omega_m L_s i_{sq}, \tag{2}$$

$$v_{sq} = R_s i_{sq} + \omega_m L_s i_{sd} + \omega_m \lambda_{fd}, \tag{3}$$

where $L_s = 13.27 \cdot 10^{-3}$H is the stator inductance, $R_s = 2.02\,\Omega$ is the stator resistance and i_{sd} is the stator current on axis d.

ω_m is related to the actual rotor speed ω_{mech}, as illustrated in Eq. (4):

$$\omega_m = \frac{N_p}{2}\omega_{mech}. \tag{4}$$

The parameter of the motor was set according to its datasheet, as shown in Table 3.

3.2. Hydraulic components

3.2.1. Bulk modulus model for fluid

For this application, the simplified Nykänen model was chosen to describe the compressibility of the hydraulic fluid [30,31]. Eq. (5) gives the bulk modulus:

$$B = \frac{\left(\left(\frac{p_0}{p}\right)^{\frac{1}{N}} X_0 + 1 - X_0\right)^2}{\frac{X_0}{Np}\left(\frac{p_0}{p}\right)^{\frac{1}{N}} + \frac{1 - X_0}{B_{liq}}}, \tag{5}$$

where p_0 is the initial pressure, p is the prevailing pressure, N is the polytropic constant, X_0 is the relative amount of free air and B_{liq} is the bulk modulus of the fluid at a specific temperature. The fluid bulk modulus, density and viscosity vary with respect to temperature by using fluid properties ISO VG 32/46 in Simulink.

3.2.2. Pump/motor model

The hydraulic gear pump/motor model for this simulation was based on Wilson's pump theory [32] by means of the least squares fitting in MATLAB.

The next six Eqs. (6)–(11) were based on the updated Wilson's pump/motor theory for variable displacement pump/motors [33]. For the purposes of this research study, since fixed displacement gear motors were selected, the displacement ratio of the pump nominal displacement included in the model is considered to be constant. From the volumetric and torque efficiency equations for the pump/motor, it can be seen that the efficiency is determined by four variables (fluid viscosity, fluid density, angular speed of the pump/motor and pressure difference across the pump/motor).

The volumetric and hydro-mechanical efficiencies of the hydraulic motor are given as follows:

$$\eta_{v\_motor} = \frac{1}{1 + \frac{C_s}{x_d S} + \frac{\Delta p}{B_{liq}} + \frac{C_{st}}{x\sigma}}, \tag{6}$$

$$\eta_{hm\_motor} = 1 - \frac{C_v S}{x_d} - \frac{C_f}{x_d} - C_h x^2 \sigma^2. \tag{7}$$

The volumetric and hydro-mechanical efficiencies of the pump are given as follows:

$$\eta_{v\_pump} = 1 - \frac{C_s}{|x_d|\ S} - \frac{\Delta p}{B_{liq}} - \frac{C_{st}}{|x_d|\ \sigma}, \tag{8}$$

$$\eta_{hm\_pump} = \frac{1}{1 + \frac{C_v S}{|x_d|} + \frac{C_f}{|x_d|} + C_h x^2 \sigma^2}, \tag{9}$$

$$S = \frac{\nu \rho \omega}{\Delta p}, \tag{10}$$

$$\sigma = \frac{\omega \sqrt[3]{V}}{\sqrt{\frac{2\Delta p}{\rho}}}, \tag{11}$$

where η_{hm_pump} and η_{hm_motor} are the hydro-mechanical efficiencies of the pump and motor; η_{v_pump} and η_{v_motor} are the volumetric efficiencies of the pump and motor; x_d is the displacement ratio of the pump/motor; Δp is the actual pressure difference over the pump/motor; ν and ρ are the actual kinematic viscosity and density of the fluid at a certain temperature; C_s and C_{st} are the coefficients of laminar and turbulent leakage of the pump; C_v, C_f and C_h are the coefficients of the viscous loss, friction loss and hydro-dynamic loss, respectively; S and σ are dimensionless numbers; and V and ω are the displacement and the actual shaft angular velocity of the pump/motor.

Fig. 9a illustrates the measured data of a motor (MGE102–630 with a displacement of 6.61 mL/r) from the manufacturer for fitting the volumetric efficiency of the pump/motor that employed the actual flow rate curve with respect to different speeds (500–4000 rpm) and two different pressures (20 bar and 250 bar) across the motor [19]. The volumetric efficiency map for the motor resolved in MATLAB using the least squares fitting method is shown in Fig. 10a, where the red points were calculated after being sampled from Fig. 9a.

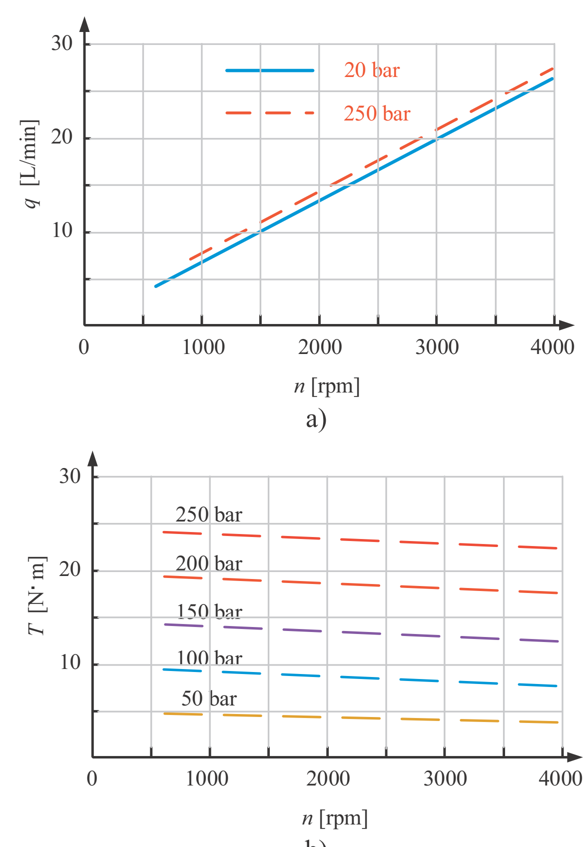

Fig. 9. Measured input flow and output torque of the motor MGE102-630 from the manufacturer [19].

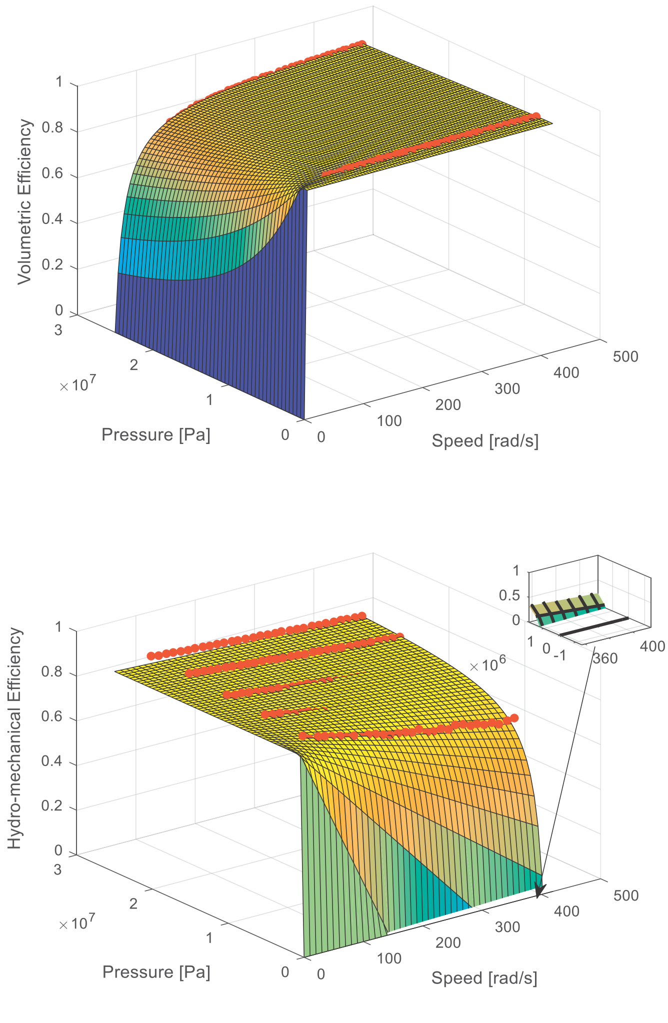

Fig. 10. Efficiency map of the motor model.

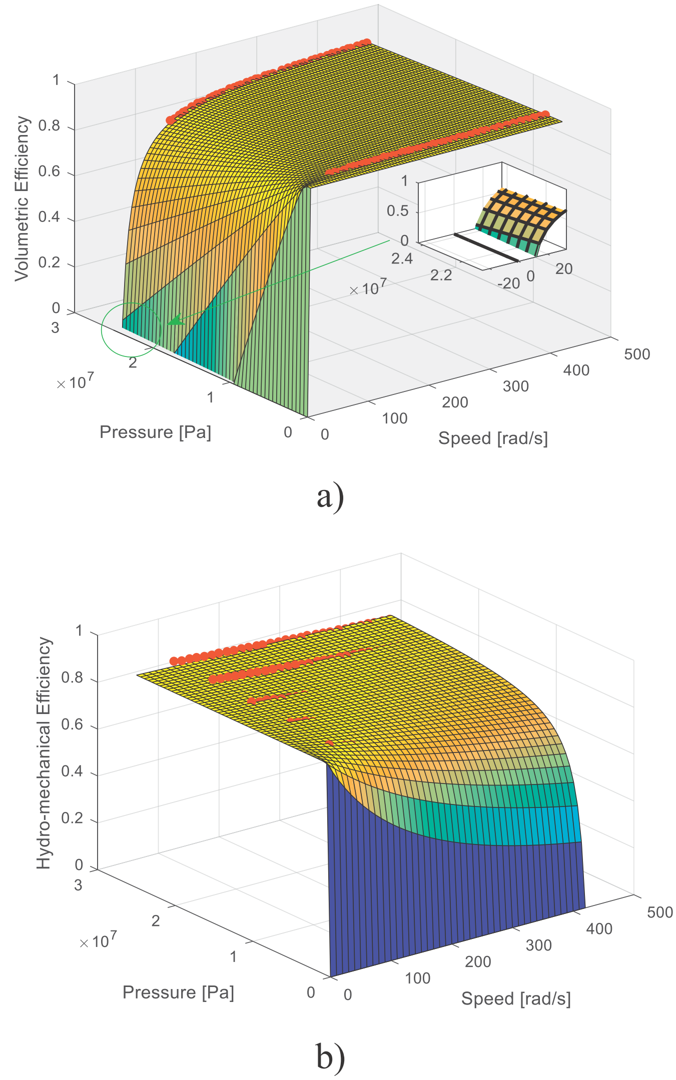

Fig. 11. Efficiency map of the pump model.

Table 4
Estimated pump/motor parameters.

Motor series	V [mL/r]	C_s	C_{st}	C_v	C_f	C_h
MGE102	6.61 4.95	2.398e−8	1.311e−4	8.935e4	0.103	0.313
MGE101	6.67 4.27	1.948e−8	1.875e−4	2.192e4	0.133	201.130

The data for fitting the hydro-mechanical efficiency of the pump/motor employed the actual torque curve with respect to different speeds (500–4000 rpm) and different pressures across the pump (50, 100, 150, 200 and 250 bar) [19], as demonstrated in Fig. 9b. Fig. 10b shows the resulting hydro-mechanical efficiency map of the motor. In addition, the estimated coefficients for Eqs. (6)–(9) are given in Table 4. It can be seen that an acceptable fitting of the experimental data point was obtained. Moreover, the dead band of the hydro-mechanical efficiency associated with the motor model is presented in the magnified figure in Fig. 10a, showing when the pressure difference is high and the angular velocity is close to zero.

Furthermore, the pump model was deduced by reusing the coefficients of the motor, as shown in Fig. 11. The magnified figure in Fig. 11a also illustrates the dead band of the volumetric efficiency associated with the pump model when the pressure difference is high and the angular velocity is close to zero. In addition, these efficiency maps of the pump/motors (MGE102 6.61 mL/r and MGE101 6.67 mL/r) have been scaled down for other pump/motors due to their belonging to the same series of HYDAC pump/motors in DDH units.

From Eq. (6), it can be seen that the leakage computation is not available when the angular velocity is zero. Therefore, the analytical model [34] of the pump was introduced to calculate the leakage when the speed of the pump/motor is zero. In this case, the leakage only depends on the differential pressure over the pump/motor.

The leakage flow rate of the pump/motor is

$$q_{\mathrm{Leak}} = K_{\mathrm{HP}} \Delta p, \tag{12}$$

where K_{HP} is the Hagen-Poiseuille coefficient for laminar pipe flow, which is determined from nominal fluid and component parameters through the following equation:

$$K_{\mathrm{HP}} = \frac{\nu_{\mathrm{Nom}}}{\rho \nu} \frac{\rho_{\mathrm{Nom}} \omega_{\mathrm{Nom}} V}{\Delta p_{\mathrm{Nom}}} (1 - \eta_{\mathrm{V,Nom}}), \tag{13}$$

where ν_{Nom} is the nominal kinematic viscosity; ρ_{Nom} is the nominal fluid density; ω_{Nom} is the nominal shaft angular velocity; Δp_{Nom} is the nominal pressure gain; and $\eta_{\mathrm{v,Nom}}$ is the volumetric efficiency with nominal condition parameters.

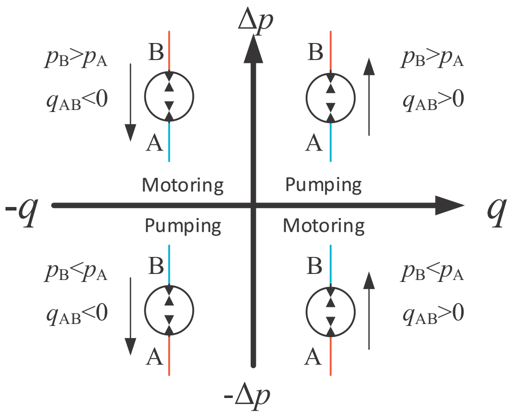

Fig. 12. Operating mode of the pump/motor.

3.2.3. Pump/motor mode switching

The possibilities of energy recovery were considered in this study. For instance, in a regenerative boom lowering movement, pump/motor B (Fig. 2) on the boom cylinder rod side was running in motoring mode, which drove the electric motor in generating mode. Thus, energy could be stored and reused at a later stage.

The pumping and motoring modes were detected by the signs of the speed and pressure differences of the four quadrant pump/motor caused by the dynamic load behaviour and the direction of movement. When they possess the same sign, the pump/motor is running in the pumping mode, otherwise it is running in the motoring mode, as demonstrated in Fig. 12. The above rule was applied to automatic switching between the volumetric model and hydro-mechanical model in the utilised simulation.

3.2.4. Hose model

The hoses and fittings were regarded as static fluid volumes. Their equations for pressure generation are described as follows in Eq. (14):

$$\dot{p}_{\mathrm{H}} = \frac{B(p)}{V_{\mathrm{H}}}(q_{\mathrm{H1}} - q_{\mathrm{H2}}), \tag{14}$$

where V_{H} is the total volume of the hose and fittings and q_{H1} and q_{H2} are the flows going into and out of the hoses and fittings.

3.2.5. Hydraulic accumulator model

Since the hydraulic accumulator operates as a low-pressure tank, the process taking place in the gas chamber in a diaphragm-type accumulator can be simplified to a reversible adiabatic process (the adiabatic constant of 1.4 for nitrogen is used), as shown in Eq. (15):

$$p_{\mathrm{a0}} = p_{\mathrm{a}} V_{\mathrm{a}}^{1.4}/V_{\mathrm{a0}}^{1.4} + p_{\mathrm{HS}}, \tag{15}$$

where p_{a0}, p_{a} and p_{HS} are the precharge pressure, the present fluid pressure and the hard-stop contact pressure, respectively. V_{a0} and V_{a} are the initial gas volume and the current gas volume.

3.2.6. Cylinder model

All three cylinders of the front attachment of the excavator have an asymmetrical design (single rod). Assuming zero piston leakage, the model describing the pressure can be divided into two individual chambers (A and B), as shown in Eqs. (16) and (17):

$$\dot{p}_{\mathrm{A}} = \frac{B(p)}{V_{0\mathrm{A}} + A_{\mathrm{A}}x}(q_{\mathrm{A}} - A_{\mathrm{A}}\dot{x}), \tag{16}$$

$$\dot{p}_{\mathrm{B}} = \frac{B(p)}{V_{0\mathrm{B}} + A_{\mathrm{A}}(x_{\max} - x)}(q_{\mathrm{B}} + A_{\mathrm{B}}\dot{x}), \tag{17}$$

where $B(p)$ is the bulk modulus of the fluid differing with its pressure; $V_{0\mathrm{A}}$ and $V_{0\mathrm{B}}$ are the dead volumes of the cylinder chambers; q_{A} and q_{B} are the flows into the A and B chambers of the cylinder; and x is the absolute position of the piston.

The piston force of the cylinder, which is coupled to the mechanical system, consists of the hydraulic force, frictional force and cylinder end force, as shown in Eq. (18):

$$F_L = (p_{\mathrm{A}}A_{\mathrm{A}} - p_{\mathrm{B}}A_{\mathrm{B}}) - F_{\mathrm{r}} - F_{\mathrm{end}}, \tag{18}$$

where the friction force F_{r} is computed by utilising the LuGre dynamic seal model [16], which is a much-used equation for describing the dependence of friction on velocity. In addition, the parameters of the seal model refer to [35], where these simulation parameters have been identified by measurements; F_{end} is the cylinder end force modelled as stiff springs and dampers.

Table 5
Definitions of power, energy and efficiency.

Equation	Symbol
$P_{\mathrm{Cyl}} = (p_{\mathrm{A}}A_{\mathrm{A}} - p_{\mathrm{B}}A_{\mathrm{B}})\cdot\dot{x}$	P_{cyl} - the output power of the cylinder, W p_{A}, p_{B} - the pressures of the piston side and rod side, Pa A_{A}, A_{B} - the effective area of the piston side and rod side, m^2 $\dot{x}\dot{x}$ - the velocity of cylinder piston, m/s
$P_{\mathrm{pump}} = T_{\mathrm{P}}\varpi_{\mathrm{P}}$	P_{pump} - the input power to the pump, W T_{P} - the torque of the pump shaft, N·m ϖ_{P} - the angular velocity of the pump shaft, rad/s
$P_{\mathrm{motor}} = T_{\mathrm{M}}\varpi_{\mathrm{M}}$	P_{motor} - the output power of the motor, W T_{M} - the torque of the motor shaft, N·m ϖ_{M} - the speed of the motor shaft, rad/s
$P_{\mathrm{ED}} = v_{\mathrm{a}}i_{\mathrm{a}} + v_{\mathrm{b}}i_{\mathrm{b}} + v_{\mathrm{c}}i_{\mathrm{c}}$	P_{ED} - the power of the electric drive, W v_{a}, v_{b}, v_{c} - the A, B and C phase voltages, V i_{a}, i_{b}, i_{c} - the A, B and C phase currents, A
$E_{\mathrm{cyl}} = \int P_{\mathrm{cyl}}\mathrm{d}t,\ (P_{\mathrm{cyl}} > 0)$	E_{cyl} - the energy input to the cylinder, J
$E_{\mathrm{po}} = \int P_{\mathrm{cyl}}\mathrm{d}t,\ (P_{\mathrm{cyl}} < 0)$	E_{po} - the potential energy input to the motor, J
$E_{\mathrm{ED}} = \int P_{\mathrm{ED}}\mathrm{d}t, (P_{\mathrm{ED}} > 0)$	E_{ED} - the energy consumed by the electric drive, J
$E_{\mathrm{reg}} = \int P_{\mathrm{ED}}\mathrm{d}t,\ (P_{\mathrm{ED}} < 0)$	E_{reg} - the energy regenerated by the electric drive, J
$E_{\mathrm{T,cyl}} = E_{\mathrm{cyl,bo}} + E_{\mathrm{cyl,ar}} + E_{\mathrm{cyl,bu}}$	$E_{\mathrm{T,cyl}}$ - the total energy input to the boom, arm and bucket cylinders, J
$E_{\mathrm{T,po}} = E_{\mathrm{po,bo}} + E_{\mathrm{po,ar}} + E_{\mathrm{po,bu}}$	$E_{\mathrm{T,po}}$ - the total potential energy input to the motors, J
$E_{\mathrm{T,ED}} = E_{\mathrm{ED,bo}} + E_{\mathrm{ED,ar}} + E_{\mathrm{ED,bu}}$	$E_{\mathrm{T,ED}}$ - the total energy input to the boom, arm and bucket electric drives, J
$E_{\mathrm{T,reg}} = E_{\mathrm{reg,bo}} + E_{\mathrm{reg,ar}} + E_{\mathrm{reg,bu}}$	$E_{\mathrm{T,reg}}$ - the total energy regenerated from the boom, arm and bucket electric drives, J
$\eta_{\mathrm{T}} = \frac{E_{\mathrm{T,cyl}}}{E_{\mathrm{T,ED}}}$	η - the total energy efficiency of the system without regeneration, %
$\eta_{\mathrm{T,reg}} = \frac{E_{\mathrm{T,cyl}}}{E_{\mathrm{T,ED}} - E_{\mathrm{T,reg}}}$	η_T - the total energy efficiency of the system when considering the regenerated energy, %

Table 6
The weight distribution of the front hoe.

	Structure [kg]	Cylinder [kg]	Others [kg]	Overall [kg]	
Boom	59.5	16.0	4.5	80.0	168.0
Arm	28.0	11.0	0	39.0	
Bucket	30.0	9.0	10.0	49.0	

3.2.7. *Definition of power distribution, energy and efficiency*

Table 5 illustrates the calculations for the power distribution, energy consumption, regeneration and efficiency of the system.

3.3. *Mechanical model*

The front hoe of the micro excavator was dissembled, and the dimensions and weights of each component were measured (Table 6). After that, a multibody model of the micro excavator was built in PTC Creo. The dimensions and weights of the selected hydraulic and mechanical components were utilised in the mechanical model of DDH units based on their specifications, including two pump/motors, one hydraulic accumulator, one electric motor, pipes and fittings, and a structure for attaching them. The weight distribution of each DDH unit is presented in Table 7.

In the full model of the excavator's front attachment, the DDH units were mounted in the existing holes of the boom and arm structures. The boom and arm DDH were symmetrically fixed to the lower part of the boom structure, and the bucket DDH was installed on the head part of the arm structure (Fig. 2).

Finally, the multibody model of this micro excavator with 3 DDH units was completed by exporting a CAD assembly from Creo software and importing it into Simscape Multibody software on the basis of the Simscape Multibody Link Creo-Pro/E plug-in.

3.4. *Full model of the excavator in Simulink*

In addition, the three DDH units, including the hydraulic, electric and control systems, were built in Simulink/MATLAB. Fig. 13 illustrates the micro excavator model with multibody and triple DDH units modelled in MATLAB/Simulink.

3.5. *Partial model validation by measurements with a standalone crane DDH*

The created DDH models were partially validated with measurements done using a one-degree-of-freedom standalone crane (Fig. 14) that used a 60/30 × 400 sized cylinder. This cylinder corresponded to the boom cylinder (60/30 × 325) of the studied excavator.

In this validation process, the measured speed of the electric drive was utilised as the input speed to the model (Fig. 15a). Furthermore, the measured and simulated cylinder positions and chamber pressures were compared in Fig. 15b and c.

The differences between the measured and simulated positions and chamber pressures show that the model has an acceptable level of accuracy. For this reason, the developed model can be utilised to evaluate the system performance of an excavator equipped with zonal hydraulics.

The following section introduces a controller design for the excavator with zonal hydraulics implemented with DDH.

Table 7
The weight distribution of the DDH units.

DDH	Weight distribution of each DDH [kg]				Overall [kg]
	Two pump/ motors	Hydraulic accumulator	Electric motor	Others	
Boom	6.6	4.0	10.0	8.4	29.0
Arm	2.4	4.0	10.0	8.4	24.8
Bucket	2.4	4.0	10.0	8.4	24.8

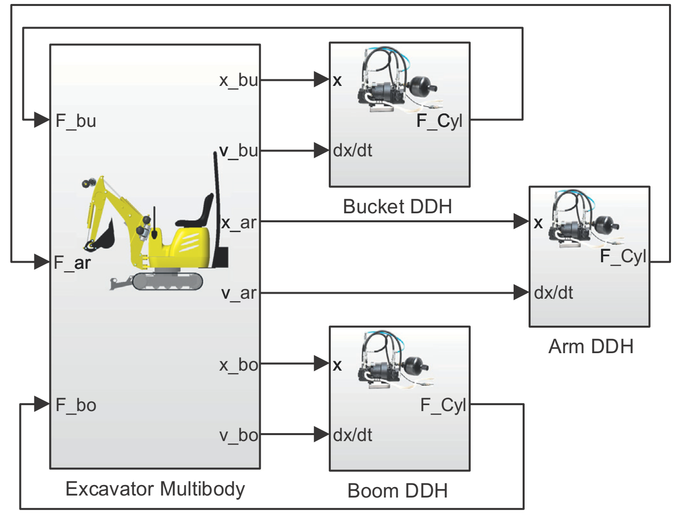

Fig. 13. Simulink model of the excavator with DDH.

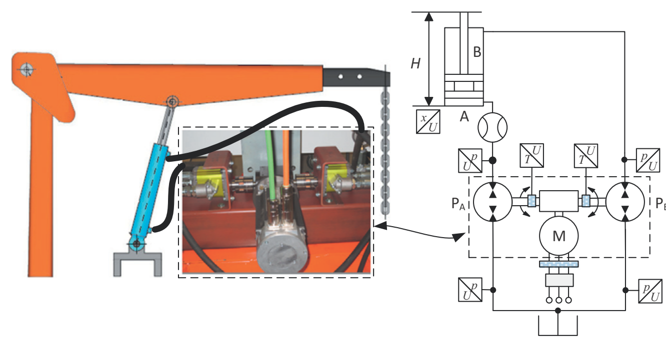

Fig. 14. DDH unit installed in one cylinder standalone crane [36].

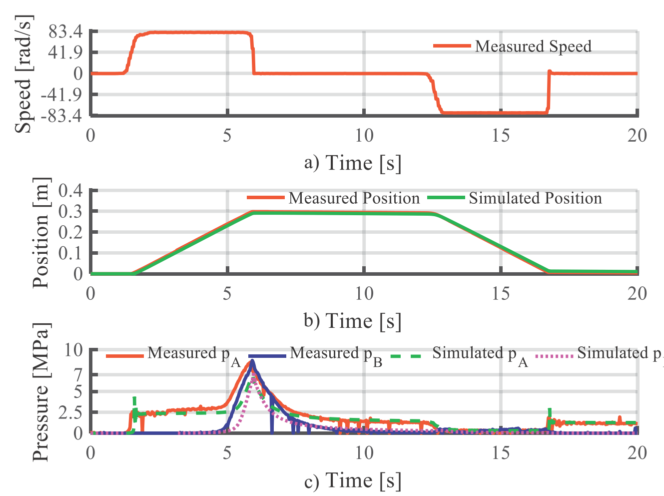

Fig. 15. Validation of simulation: a) input speed, b) position tracking and c) pressures of chambers A and B [26].

4. Controller design

To achieve a balance between high energy efficiency and good performance, the control design of the DDH has to be optimised based on the operational requirements for the excavator. In this paper, a

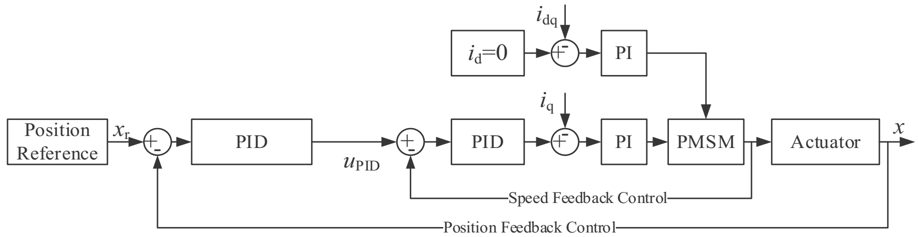

Fig. 16. Control schematics of the DDH with PID.

conventional proportional-integral-derivative (PID) controller and a feedforward control (FFC) plus PID were used to study the combined energy efficiency and control performance of a DDH-based excavator in different work cycles with varying operational requirements. One aim of the controller design is that the actuator can follow the desired trajectory accurately and smoothly. Therefore, the tracking error is regarded as the main objective of the targeted control performance. Another aim of the controller design is to maintain a low energy consumption and high energy efficiency of the whole DDH system. Therefore, the energy consumption and energy efficiency will be calculated for all the selected work cycles.

4.1. Conventional PID control

Fig. 16 illustrates the overall control schematics of one DDH unit, where the speed control of the electric motor and position control of the cylinder both adopted the conventional PID control.

The input to the controller is the error between the actual position and the position reference, where Kp, K_i and K_d are the proportional, integral and derivative gains, respectively. The control parameters of PID were calculated using the Zielgr-Nichols method and fine-tuned manually.

4.2. Feedforward plus PID based on flow rate matching

This section describes the application of a feedforward velocity compensation approach based on the flow-rate-matching model for the pump and cylinder.

Considering the strong changing external force of the actuators during the combined motion of three actuators, the DDH position control using a conventional PID regulator was not as good as expected. To achieve good tracking performance, a feedforward controller (FFC) was used in addition to the position feedback PID controller. The feedforward input u_{ffc} commands a flow rate corresponding to the desired velocity. It should be noted that the major function of the position feedback controller is to regulate against the changing of the load, leakage of the pump/motors and any modelling error. The feedforward controller is not sensitive to the changing force and can give a control signal in advance according to the desired position over the time signal. Therefore, the position error, which needs to be tuned by the PID controller, can be significantly reduced; thus, the rapidity and accuracy of the position control will increase.

Fig. 17 illustrates the overall control schematics of the DDH unit, where the speed control of the electric motor and position control of the cylinder adopt conventional PID control and FFC plus PID control, respectively.

FFC can produce an initial control signal to match the desired control signal, and thus, decrease the correction from the PID controller and improve the position tracking performance. For a cylinder, its demanded flow rate is the product of its corresponding area and velocity, as shown in Eqs. (19) and (20),

$$q_{\mathrm{Cyl\_A}} = \dot{x}A_{\mathrm{A}}, \tag{19}$$

$$q_{\mathrm{Cyl\_B}} = \dot{x}A_{\mathrm{B}}. \tag{20}$$

For the pump/motors A or B running in the pumping mode, as shown in Eqs. (21) and (22), the produced effective flow rate is determined by the pump's actual flow rate, namely the product of its rotational speed and displacement, minus its leakage, which is mainly caused by the pressure difference over it. For the motoring mode, the required flow rate is the product plus the leakage. Since the percentage of the leakage flow divided by the flow rate is relatively small (usually down to 10%) and varies with pressure across the pump/motor and rotational speed, the leakage effect was not considered when calculating the feedforward control signal in Eq. (23):

$$q_{\mathrm{PM\_A}} = \begin{cases} nV_{\mathrm{PM\_A}} - q_{\mathrm{P,leakage}} & \text{pumping} \\ nV_{\mathrm{PM\_A}} + q_{\mathrm{M,leakage}} & \text{motoring}' \end{cases} \tag{21}$$

$$q_{\mathrm{PM\_B}} = \begin{cases} nV_{\mathrm{PM\_B}} - q_{\mathrm{P,leakage}} & \text{pumping} \\ nV_{\mathrm{PM\_B}} + q_{\mathrm{M,leakage}} & \text{motoring}' \end{cases} \tag{22}$$

$$u_{\mathrm{FFC}} = \frac{\dot{x}A_{\mathrm{A}}}{V_{\mathrm{PM\_A}}} \approx \frac{\dot{x}A_{\mathrm{B}}}{V_{\mathrm{PM\_B}}}. \tag{23}$$

5. Results and analysis

Simulations of the DDH-equipped excavator were carried out with three groups of desired trajectories using a conventional PID control and an FFC plus PID control. The trajectories included a typical digging cycle, a JCMAS digging cycle and a JCMAS levelling cycle. During the simulation of the three cycles, only one set of parameters was used for PID control and FFC plus PID control, respectively.

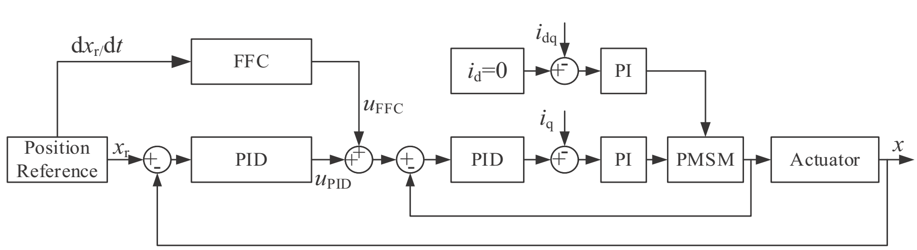

Fig. 17. Control schematics of feedforward plus PID controller.

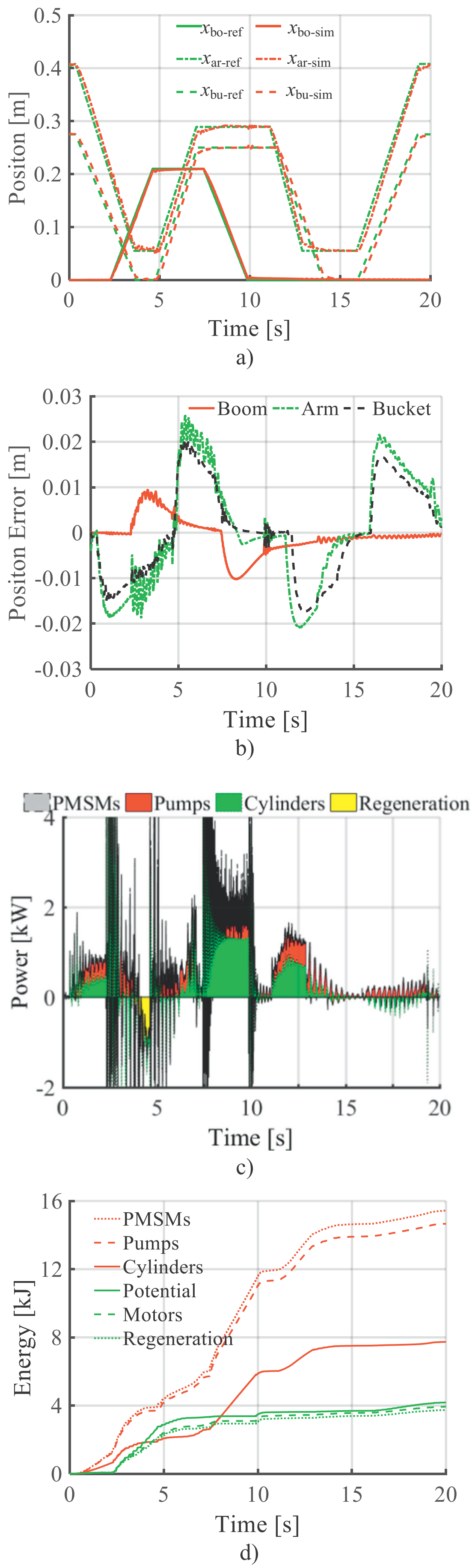

Fig. 18. Simulation results for a digging cycle with the PID controller: a) position output, b) position tracking error, c) power distribution, d) energy consumption.

5.1. Typical digging cycle

This subsection presents the simulations of a typical digging cycle. The results include the tracking performance and energy consumption with the two alternative controls.

Figs. 18a and 19a show the desired typical digging trajectories and the simulated trajectories for the boom, arm and bucket DDH. Figs. 18b and 19b demonstrate the tracking errors for the two controllers.

It can be seen that the FFC plus PID controller is better than the PID controller in a typical digging cycle from a position tracking performance angle. Table 8 shows the root mean square tracking errors and the maximum tracking errors for the two controllers. The proportional and integral control constants of the PID controller were quite high, but the rapidity performance of the PID controller was still no better than that with the FFC plus PID controller. The range of root mean square tracking errors with the PID controller and the FFC plus PID controller were from 5.0 mm to 10.2 mm and from 0.7 mm to 2.1 mm, respectively. The root mean square tracking errors reduced by at least 74%. Additionally, the max tracking error decreased by at least 50%—from 10.2 mm to 3.3 mm, from 25.8 mm to 7.8 mm and from 20.2 mm to 10.1 mm for the boom, arm and bucket cylinder, respectively, when the PID controller was replaced with the FFC plus PID controller.

Figs. 18c and 19c present the power distribution of the cylinders, pump/motors, PMSMs and regeneration. In the regeneration area, the pump/motors ran in the motoring mode and the PMSMs ran in the generating mode. Therefore, regeneration of potential energy was possible for the DDH units during the boom lowering phase. Furthermore, Figs. 18d and 19d illustrate the energy consumption when using the two controls. Fig. 19e illustrates the rotating speeds of the three electric motors with the FFC plus PID controller in a typical digging cycle.

Table 9 compares the energy consumption and efficiency with the two controllers. The energy consumed by a typical digging cycle with the PID controller was 22% (2.2 kJ) higher than that with an FFC plus PID controller because there were heavier oscillations caused by the high proportional and integral controller constants of the PID controller. Additionally, the energy efficiencies of the two controllers were 50.1% and 60.5%, respectively, without regeneration.

In this simulation, when the boom and arm lowering, the potential and braking energy of them was recovered. The regenerated energies were 3.7 kJ and 2.1 kJ for the PID controller and the FFC plus PID controller, respectively. The reason for higher energy regeneration from the cycle with the PID controller was higher oscillations, as shown in Fig. 18c. Even with the higher recovered energy produced by the oscillations, the overall efficiency of the cycle with the PID controller (65.8%) was still 8.4% units lower than that with the FFC plus PID controller (74.2%), as shown in Table 9.

Since the regeneration possibility and cumulative energy of the components of the DDH units have already been shown for the typical digging cycle, the figures for the power distributions and energy consumption of the JCMAS digging and level cycles have been omitted in the next two subsections.

5.2. JCMAS digging cycle

In this subsection, the simulations were performed using the two proposed controllers with the JCMAS digging cycle. Figs. 20 and 21 present the position tracking and the tracking error of the digging cycle with the PID controller and the FFC plus PID controller. Additionally, Fig. 21c shows the rotational speeds of the three electric motors of the cycle with the FFC plus PID controller.

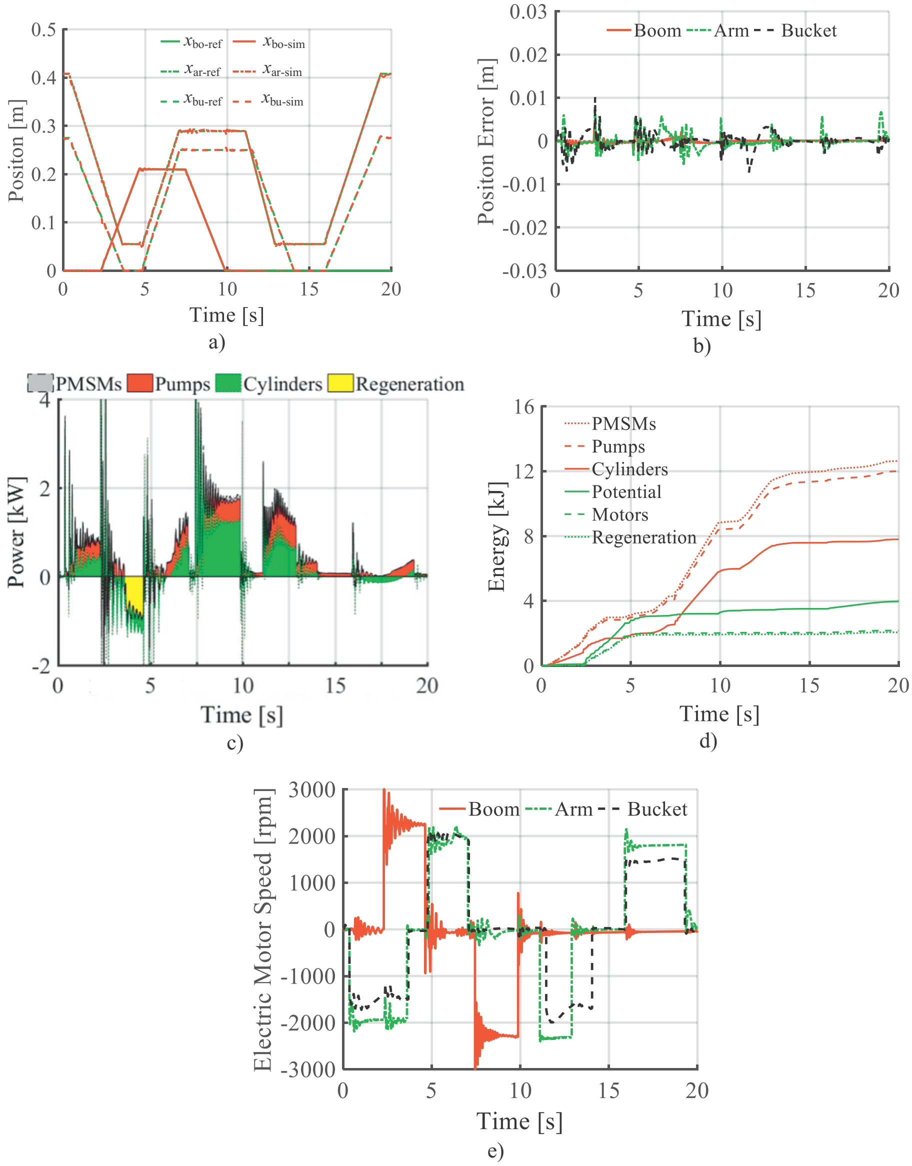

Fig. 19. Simulation results for the digging cycle with the FFC plus PID controller: a) position output, b) position tracking error, c) power distribution, d) energy consumption, e) electric motor speed.

Table 8
Tracking errors for both controllers with a typical cycle.

Control method	Root mean square tracking error and max error [10^{-3}m] of the different functions					
	Boom		Arm		Bucket	
PID	5.0	10.2	10.2	25.8	8.1	20.2
FFC + PID	0.7	3.3	2.1	7.8	2.1	10.1

Table 9
Energy efficiency and consumption comparison with a typical digging cycle.

Control method	Input $E_{T,\ ED}$ [kJ]	Output $E_{T,\ cyl}$ [kJ]	Efficiency η_T [%]	Regeneration $E_{T,\ reg}$ [kJ]	Efficiency $\eta_{T,\ reg}$ [%]
PID	15.4	7.7	50.1	3.7	65.8
FFC + PID	12.6	7.8	61.5	2.1	74.2

Table 10 presents the root mean square tracking errors and the maximum tracking errors for the two controllers after calculations. As it was with typical digging, the FFC plus PID controller was also better than the PID controller in the JCMAS digging cycle. Although the proportional and integral controller constants of the PID controller were quite high, the rapidity of the PID controller was still not as good as the FFC plus PID controller, especially where the arm and bucket cylinders were being retracted with a changing load produced by the fast lifting of the arm and bucket. Therefore, the tracking errors of the PID controller were much higher.

Table 11 compares the energy consumptions of the two controllers. It can be seen that more energy was consumed with the PID controller, and the efficiencies of this controller both with and without regeneration were approximately 24.5% and 28.4% lower than with the FFC plus PID controller.

5.3. JCMAS levelling cycle

In this subsection, the simulations were performed using the two proposed controllers with the JCMAS levelling cycle. Figs. 22 and 23

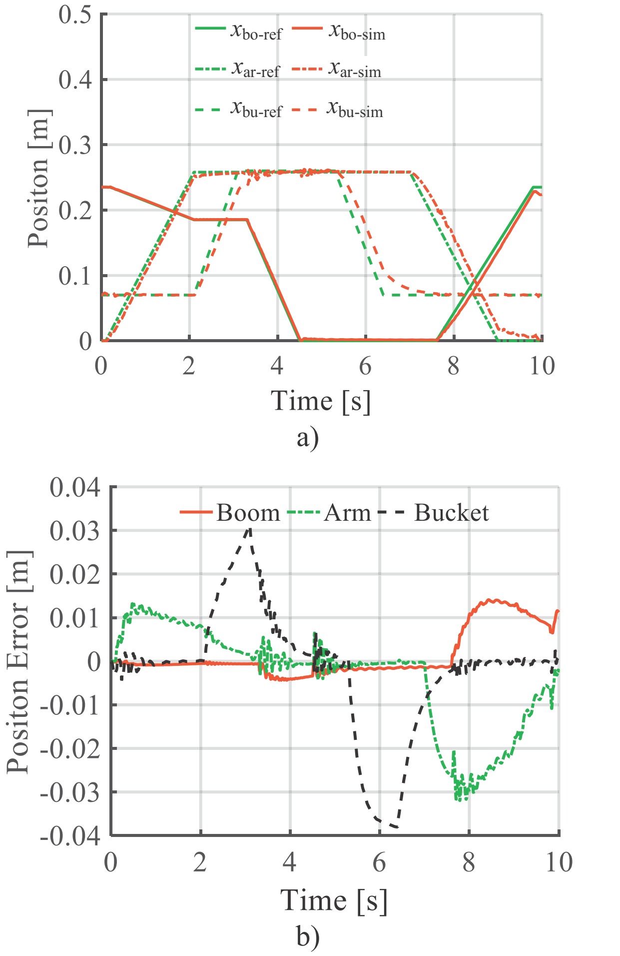

Fig. 20. Simulation results for the JCMAS digging cycle with PID controller: a) position output and b) position tracking error.

present the position tracking and the tracking errors of the JCMAS levelling cycle with the PID controller and the FFC plus PID controller. Furthermore, Fig. 23c demonstrates the rotational speeds of the three electric motors in the cycle.

The tracking performance of bucket DDH was omitted because its cylinder was held in levelling cycle. Table 12 shows the root mean square tracking errors and the maximum tracking errors with the two controllers. Again, the feedforward plus PID controller was better than the PID controller in the JCMAS levelling cycle. The maximum error of the arm DDH reached 40.3 mm with the PID controller, which was caused by the demanded high lifting speed, the insufficient proportional gain and the integral gain. By contrast, the maximum tracking error achieved with the FFC plus PID controller had an acceptable value of 6.6 mm.

Table 13 compares the energy consumptions of the two controllers. It shows that less energy was consumed with the FFC plus PID controller, which improved the system's energy consumption by > 12% compared with the PID controller.

6. Discussion

The purpose of this case study was to investigate the effects of the control methods on the energy efficiency and tracking performance of an electro-hydraulic excavator with zonal hydraulics based on a MATLAB/Simulink model that included three DDH units and one multibody.

In this simulation model, the hydraulic gear pump/motor volumetric and hydro-mechanical efficiency models, which were both built

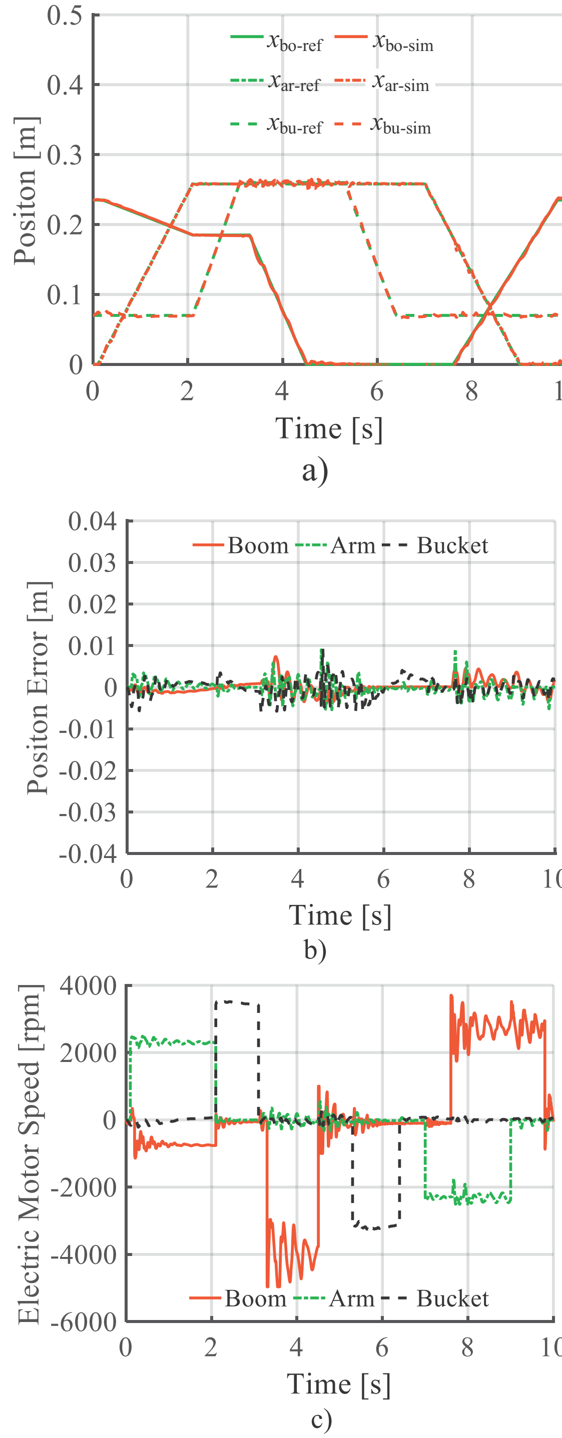

Fig. 21. Simulation results for the JCMAS digging cycle with FFC plus PID controller: a) position output, b) position tracking error and c) electric motor speed.

based on Wilson's pump theory by means of the least squares fitting method using measurements from the manufacturer, took into account not only the pressure differences across the pump/motor, but also the angular velocities of the pump/motor shaft. Seal models of all three cylinders were identified via the experiment with the micro excavator. Further, the created DDH models were partially validated with measurements done with a one-degree-of-freedom standalone crane. The variable speed of the electric motor with servo drive that drives the hydraulic pump/motors of the DDH unit is one of its most critical

Table 10
Tracking errors for both controllers with the JCMAS digging cycle.

Control method	Root mean square tracking error and max error [10^{-3} m] of the different functions					
	Boom		Arm		Bucket	
PID	4.7	14.1	11.5	32.0	8.0	38.1
FFC + PID	1.8	7.4	2.0	9.1	2.4	9.3

Table 11
Energy efficiency and consumption comparison with the JCMAC digging cycle.

Control method	Input $E_{T,\ ED}$ [kJ]	Output $E_{T,\ cyl}$ [kJ]	Efficiency η_T [%]	Regeneration $E_{T,\ reg}$ [kJ]	Efficiency $\eta_{T,\ reg}$ [%]
PID	14.5	5.9	40.9	3.9	55.7
FFC + PID	10.6	6.9	65.4	2.4	84.1

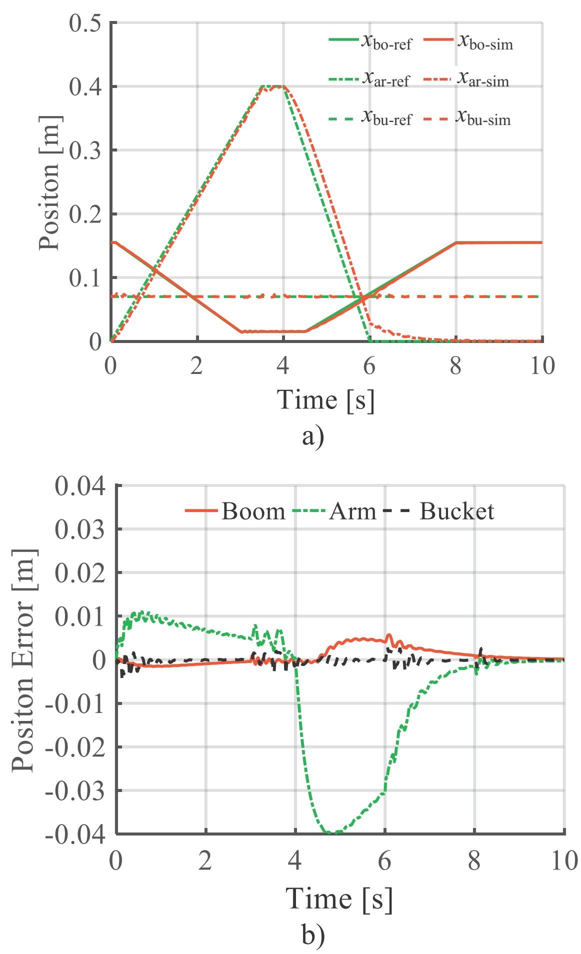

Fig. 22. Simulation results for the JCMAS levelling cycle with the PID controller: a) position output, b) position tracking error and c) motor speed.

components from an actuator control angle. In this paper, the efficiency of the electric motor was set at a constant 95%, which will be replaced with dynamic efficiency depending on the rotational speed and torque in the next phase of the study.

Simulations of the excavator equipped with zonal hydraulics were performed by adopting the proposed flow-rate-matching-based FFC plus PID controller and the conventional PID controller with various working cycles, including the typical digging with varying payload, the JCMAS digging without payload and the JCMAS levelling in the air. In

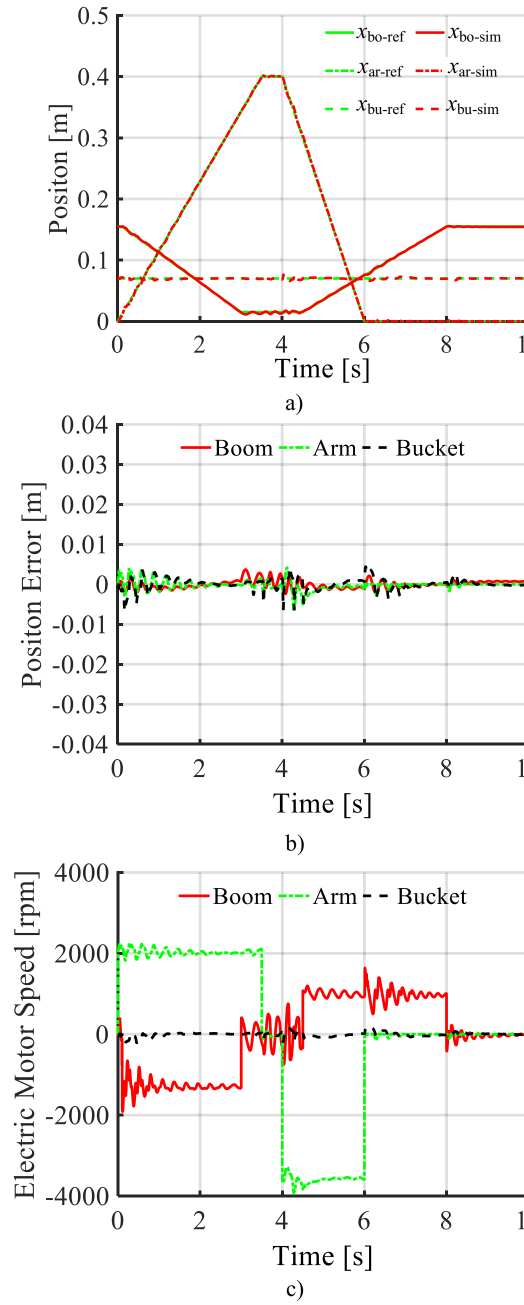

Fig. 23. Simulation results for the JCMAS levelling cycle with FFC plus PID controller: a) position output, b) position tracking error and c) electric motor speed.

Table 12
Tracking errors for both controllers with the JCMAS levelling cycle.

Control method	Root mean square tracking error and max error [10^{-3} m] of the different functions			
	Boom		Arm	
PID	1.5	5.7	12.6	40.3
FFC + PID	1.2	3.7	1.6	6.6

Fig. 24a, the results demonstrate that the proposed FFC plus PID controller yields better tracking results than the PID controller (the root mean square tracking errors lowered by 20–87%), reducing the maximum tracking error significantly (the maximum errors lowered by

Table 13
Energy efficiency and consumption comparison with JCMAS levelling cycle.

Control method	Input $E_{T,\ ED}$ [kJ]	Output $E_{T,\ cyl}$ [kJ]	Efficiency η_T [%]	Regeneration $E_{T,\ reg}$ [kJ]	Efficiency $\eta_{T,\ reg}$ [%]
PID	7.4	3.2	43.2	1.9	58.1
FFC + PID	6.3	3.6	57.1	1.5	75.0

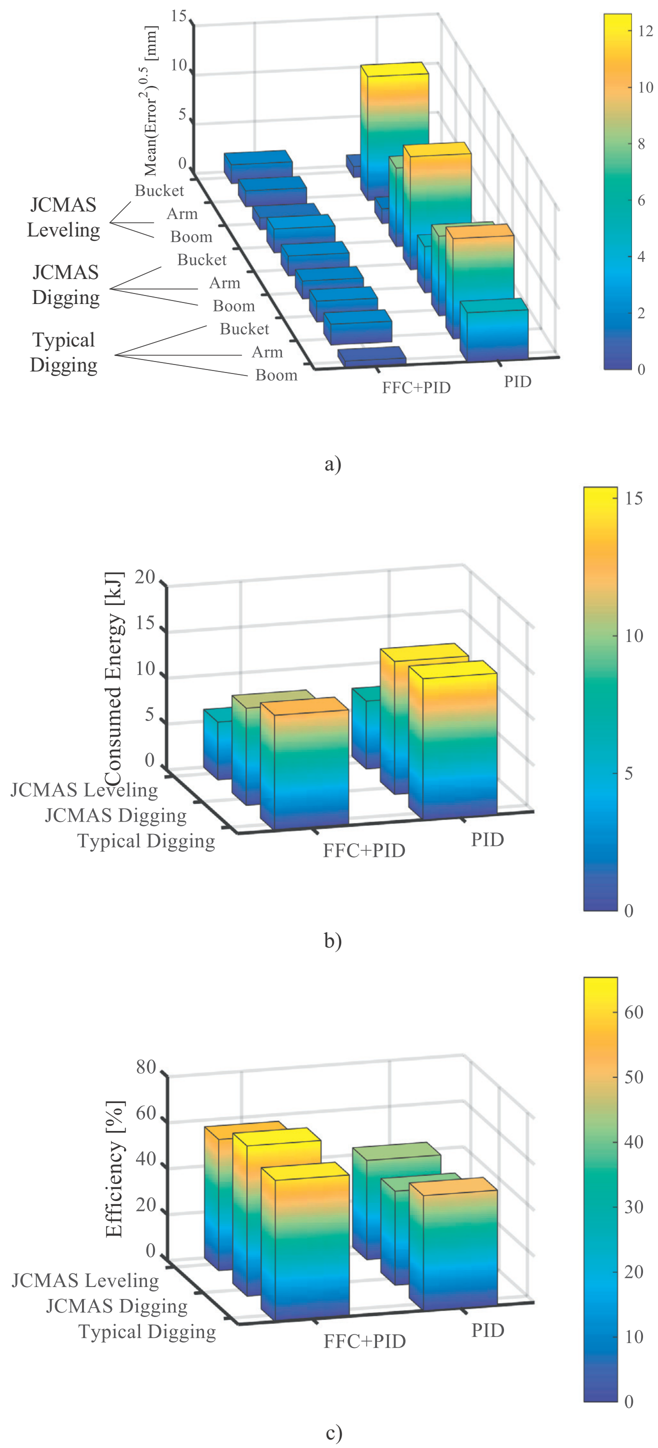

Fig. 24. Comparison of the two controllers with different cycles: a) root mean square errors of the position tracking, b) consumed energy without regeneration and c) energy efficiency without regeneration.

35–83%) and following the desired position more accurately. Fig. 24b and c in turn show that the energy consumption of the excavator was significantly lower and the system efficiency correspondingly noticeably higher with the FFC plus PID controller compared to the PID controller. The efficiency of the excavator can be improved by 11–24% without regeneration and by 8–28% when considering regeneration by switching the controller from a conventional PID controller to the proposed FFC plus PID controller.

During digging cycles with and without payload, and also during the levelling cycle, multiple cylinders operate simultaneously, which means a changing load acting on the cylinders. In this case, the tracking of the desired position meant not only tracking performance, but also the ability of the controller to overcome external disturbances.

The drawback of the proposed system is that the overall costs would increase to some extent, since each DDH unit requires one variable-speed electric motor with one servo drive, one hydraulic accumulator and one pair of fixed displacement pump/motors. In addition, the DDH units bring additional loads to each working cycle of the system, and thus, increase energy consumption, as they are mounted on the moving front attachments of the excavator, namely the moving boom and arm. However, the advantages stated in the introductory section outweigh these drawbacks for many applications.

7. Conclusion

The presented work concentrated on analysing the possible improvements in an electro-hydraulic micro excavator with the application of zonal hydraulics. The efficiency behaviour for electro-hydraulic zonal system components and the cycle efficiencies of the DDH systems were determined. It was shown that controller design affects the efficiency of the studied case excavator due to direct control by an electric servo drive.

The results demonstrated that the proposed FFC plus PID controller benefits the micro excavator from an energy standpoint when having the proposed zonal configuration. Efficiencies of the excavator can be improved by 11–24% without regeneration and by 8–28% when considering regeneration, and the energy consumption can be reduced by at least 15% without regeneration and by at least 10% with regeneration by switching from a conventional PID controller to the proposed flow-rate-matching FFC plus PID controller. At the same time, better position tracking performance was achieved, and the simulation results illustrate that the root mean square tracking error and maximum errors were lowered by 20–87% and 35–83%, respectively.

Based on the simulations of three work cycles, it can be concluded that the flow-rate-matching FFC plus PID controller yields better tracking results than the conventional PID controller, thereby reducing position tracking errors significantly. At the same time, the energy consumption of the excavator decreased noticeably and the efficiency of the system increased remarkably. The combination of lower energy consumption and the accurate position control of zonal hydraulics has universal significance in terms of facilitating the electrification and automatisation of construction machinery and off-road machinery in general. The presented results can be applied to construction machinery such as hydraulic excavators, loaders, forest harvesters and other industrial stationary applications possessing similar working conditions.

A further step in the research will entail an experimental validation of the proposed models and efficiencies, as the determined efficiencies were based on combining the manufacturer's curves, measurement of a conventional electro-excavator and modelling results validated in a stand-alone experimental setup. In order to improve tracking performance and efficiency, solutions such as adding a low pressure compensation unit for multiple DDH units, optimising the component parameters and the location of the DDH units will be a part of future investigations and studies of FFC plus PID controllers in a micro excavator.

Nomenclature

A	Area [m^2]
B	Bulk modulus [Pa]
C_f	Friction loss coefficient [-]
C_h	Hydro-dynamic loss coefficient [-]
C_s	Laminar leakage coefficient [-]
C_{st}	Turbulent leakage coefficient [-]
C_v	Viscous loss coefficient [-]
E	Energy [J]
F_i	Force [N]
$i_{a,b,c}$	Phase current [A]
i_{sq}	Stator current in q axis [A]
i_{sd}	Stator current in d axis [A]
L_s	Stator inductance [mH]
n	Rotational speed [rev/s]
N_p	Number of pole pairs [-]
$p_{A,B}$	Pressure [Pa]
P	Power [W]
q	Flow rate [m^3/s]
$R_{ideal,\ derivation}$	Displacement ratio of two pump/motors B and A [-]
R_s	Stator resistance [Ω]
S	Dimensionless number [-]
$v_{a,b,c}$	Phase voltage [V]
V	Displacement of the pump [m^3/rev]
x	Displacement of the cylinder [m]
x_d	Displacement ratio of the pump/motor [-]
η	Efficiency [-]
λ_{fd}	Flux linkage of the stator d winding [$kg{\cdot}m^2{\cdot}s^{-2}{\cdot}A^{-1}$]
υ	Kinematic viscosity [mm^2/s]
ρ	Density of the fluid [kg/m^3]
σ	Dimensionless number [-]
ω_m	Angular velocity [rad/s]
ω_{mech}	Actual rotor velocity [rad/s]

Abbreviation

DDH	Direct Driven Hydraulics
PMSM	Permanent magnet synchronous motor
PID	Proportional-integral-derivative
FFC	Feedforward control
JCMAS	Japan Construction Mechanization Association

Acknowledgments

This work was enabled by the financial support of Business Finland (the Finnish Funding Agency for Innovation (former TEKES), project EL-Zon) and the Academy of Finland (IZIF project, No. 304943) and internal funding from the Department of Mechanical Engineering at Aalto University, Finland. Additionally, the work was supported by the Natural Science Foundation of Fujian Province, China (No. 2016J01203), the Scientific Research Fund of Fujian University of Technology, China (No. GY-Z15096) and the Public Service Platform for Technical Innovation of Machine Tool Industry of Fujian Province, China.

References

[1] P. Casoli, L. Riccò, F. Campanini, et al., Hydraulic hybrid excavator—mathematical model validation and energy analysis, Energies 9 (12) (2016), https://doi.org/10.3390/en9121002.

[2] T. Lin, W. Huang, H. Ren, et al., New compound energy regeneration system and control strategy for hybrid hydraulic excavators, Autom. Constr. 68 (2016) 11–20, https://doi.org/10.1016/j.autcon.2016.03.016.

[3] H. Kim, S. Yoo, S. Cho, et al., Hybrid control algorithm for fuel consumption of a compound hybrid excavator, Autom. Constr. 68 (2016) 1–10, https://doi.org/10.1016/j.autcon.2016.03.017.

[4] H. Wang, Q. Wang, B. Hu, A review of developments in energy storage systems for hybrid excavators, Autom. Constr. 80 (2017) 1–10, https://doi.org/10.1016/j.autcon.2017.03.010.

[5] J. Breen, JCB'S first 'electric' excavator breaks ground, https://www.agriland.ie/farming-news/jcbs-first-electric-excavator-breaks-ground/, (2018) , Accessed date: 20 April 2018.

[6] Sennebogen, Electric excavator, https://www.sennebogen.com/en/products/electric-excavator.html, (2018) , Accessed date: 22 April 2018.

[7] Volvo, Volvo Ce unveils 100% electric compact excavator prototype, https://www.volvoce.com/global/en/news-and-events/news-and-press-releases/volvo-ce-unveils-100-percent-electric-compact-excavator-prototype/, (2017) , Accessed date: 20 April 2018.

[8] J. Shi, L. Quan, X. Zhang, et al., Electro-hydraulic velocity and position control based on independent metering valve control in mobile construction equipment, Autom. Constr. 94 (2018) 73–84, https://doi.org/10.1016/j.autcon.2018.06.005.

[9] X. He, Y. Jiang, Review of hybrid electric systems for construction machinery, Autom. Constr. 92 (2018) 286–296, https://doi.org/10.1016/j.autcon.2018.04.005.

[10] L. Ge, L. Quan, X. Zhang, et al., Efficiency improvement and evaluation of electric hydraulic excavator with speed and displacement variable pump, Energy Convers. Manag. 150 (2017) 62–71, https://doi.org/10.1016/j.enconman.2017.08.010.

[11] T. Lin, L. Wang, W. Huang, et al., Performance analysis of an automatic idle speed control system with a hydraulic accumulator for pure electric construction machinery, Autom. Constr. 84 (2017) 184–194, https://doi.org/10.1016/j.autcon.2017.09.001.

[12] S. Dadhich, U. Bodin, U. Andersson, Key challenges in automation of earth-moving machines, Autom. Constr. 68 (2016) 212–222, https://doi.org/10.1016/j.autcon.2016.05.009.

[13] S. Zhang, T. Minav, M. Pietola, Decentralized Hydraulics for Micro Excavator, The 15th Scandinavian International Conference on Fluid Power, Linköping, Sweden, June 7–9, (2017), https://doi.org/10.3384/ecp17144187.

[14] T. Minav, T. Lehmuspelto, P. Sainio, et al., Series Hybrid Mining Loader with Zonal Hydraulics, 10th International Fluid Power Conference, Dresden, Germany, 8–10 March, 2016, http://nbn-resolving.de/urn:nbn:de:bsz:14-qucosa-196676 , Accessed date: 25 May 2018.

[15] T. Hassi, A. Korva, S. Markkula, et al., Improving Energy Efficiency of an Electric Mini Excavator, International DAAAM Baltic Conference, Industrial Engineering, Tallinn, Estonia, 2016 20-22 April. ISBN: 978994923987 http://innomet.ttu.ee/daaam/proceedings/Mechatronics/Hassi.pdf , Accessed date: 19 March 2018.

[16] A. Järf, Flow compensation using hydraulic accumulator in direct driven hydraulic differential cylinder application and effects on energy efficiency, Aalto University, Espoo, Finland, 2016http://urn.fi/URN:NBN:fi:aalto-201605262260 , Accessed date: 1 January 2018Master Thesis.

[17] A. Järf, T. Minav, M. Pietola, Nonsymmetrical Flow Compensation Using Hydraulic Accumulator in Direct Driven Differential Cylinder Application, Proceedings of the ASME 2016 9th FPNI Ph.D. Symposium on Fluid Power, Florianópolis, SC, Brazil, Oct. 26–28, (2016), https://doi.org/10.1115/FPNI2016-1516.

[18] N.D. Manring, S.B. Kasaragadda, The theoretical flow ripple of an external gear pump, J. Dyn. Syst. Meas. Control. 125 (3) (2003) 396–404, https://doi.org/10.1115/1.1592193.

[19] HYDAC International, Motor specifications, https://www.hydac.com/fileadmin/pdb/pdf/PRO000000000000000000029021000011.pdf, (2016) , Accessed date: 7 February 2017.

[20] Bosch Rexroth, Diaphragm-type accumulator revision, http://dc-america.resource.bosch.com/media/us/products_13/product_groups_1/industrial_hydraulics_5/pdfs_4/re50150.pdf, (2013) , Accessed date: 30 December 2016.

[21] M. Fecke, Standardisierung Definierter Lastzyklen Und Messmethoden Zur Energieverbrauchsermittlung Von Baumaschinen, Proceedings of the 5th Fachtgaung Baumaschinentechnik, Dresden, Germany, 17–19, September, 2015, https://doi.org/10.2314/GBV:86993631X.

[22] C. Holländer, Untersuchungen Zur Beurteilung Und Optimierung Von Baggerhydrauliksystemen, Ph.D. Thesis TU Braunschweig, Braunschweig, Germany, 3183307014, 1998https://books.google.com/books?id=GcWEAAAACAAJ&source=gbs_navlinks_s , Accessed date: 21 June 2017.

[23] J.D. Zimmerman, M. Pelosi, C.A. Williamson, Energy Consumption of an Ls Excavator Hydraulic System, ASME International Mechanical Engineering Congress &Exposition, Seattle, Washington, USA, November 11–15, 2007, (2007), https://doi.org/10.1115/IMECE2007-42267.

[24] JCMAS H020, Earth-Moving Machinery—Fuel Consumption On Hydraulic Excavator—Test Procedures, Tokyo, Japan, Japan Construction Mechanization Association, 2007http://www.cema.or.jp/general/news/pdf/17th/17thJapanese.pdf , Accessed date: 15 May 2018.

[25] S. Mieth, S. Voigt, G. Kunze, Typical Performance Cycles of Mobile Machinery Taking Into Account the Operator Influence, 8th International Fluid Power Conference, Dresden, Germany, 26–28 March, https://books.google.nl/books?id=0sRGmwEACAAJ, (2012) , Accessed date: 19 March 2018.

[26] S. Zhang, T. Minav, M. Pietola, Improving Efficiency of Micro Excavator with Decentralized Hydraulics, ASME/BATH 2017 Symposium on Fluid Power and Motion Control, Sarasota, Florida, USA, 2017, 8 (2017), https://doi.org/10.1115/FPMC2017-4341 V1T. Accessed.

[27] G.I. Ofoegbu, R.S. Read, F. Ferrante, Bulking factor of rock for underground openings, https://www.nrc.gov/docs/ML0807/ML080700314.pdf, (2008) , Accessed date: 15 April 2017.

[28] N. Mohan, Advanced Electric Drives: Analysis, Control, and Modeling Using MATLAB/Simulink, John Wiley & Sons, Inc., Hoboken, New Jersey, 111891113X, 2014.

[29] Emerson Industrial Automation, Technical data unimotor FM and HD high

performance AC brushless servo motors, http://www.emersonindustrial.com/en-en/documentcenter/ControlTechniques/Brochures/unimotor_technical_data.pdf, (2013) , Accessed date: 22 January 2018.
[30] H. Gholizadeh, D. Bitner, R. Burton, et al., Modeling and experimental validation of the effective bulk modulus of a mixture of hydraulic oil and air, J. Dyn. Syst. Meas. Control. 136 (5) (2014) 1–14, https://doi.org/10.1115/1.4027173.
[31] T. Nykänen, S. Esque, A. Ellman, Comparison of Different Fluid Models, Bath Workshop on Power Transmission and Motion Control (PTMC 2000), Bath, UK, (2000) 1860582648, pp. 101–110.
[32] A. Pourmovahed, N.H. Beachley, F.J. Fronczak, Modeling of a hydraulic energy regeneration system: part I—analytical treatment, J. Dyn. Syst. Meas. Control. 114 (1) (1992) 155–159, https://doi.org/10.1115/1.2896497.
[33] N.H. Beachley, F.J. Fronczak, Modeling of a hydraulic energy regeneration system-Part I: analytical treatment, J. Dyn. Syst. Meas. Control. 114 (1992) 155, https://doi.org/10.1115/1.2896497.
[34] The MathWorks Inc., Fixed-displacement pump, https://se.mathworks.com/help/physmod/hydro/ref/fixeddisplacementpump.html, (2016) , Accessed date: 25 March 2017.
[35] V. Salomaa, Efficiency Study of an Electro-Hydraulic Excavator, Master Thesis Tampere University of Technology, Tampere, Finland, 2017http://URN.fi/URN:NBN:fi:tty-201709201904 , Accessed date: 10 September 2017.
[36] T. Minav, S. Zhang, M. Pietola, Eliminating sizing error in direct-driven hydraulics, The 10th JFPS International Symposium on Fluid Power, Fukuoka, Japan, 24–27 October, 2017 https://confit.atlas.jp/guide/event-img/jfps2017/1A09/public/pdf?type=in , Accessed date: 19 March 2018.